NOTES AND CORRESPONDENCE

Is the Faroe Bank Channel Overflow Hydraulically Controlled?

JAMES B. GIRTON

Applied Physics Laboratory, University of Washington, Seattle, Washington

LAWRENCE J. PRATT, DAVID A. SUTHERLAND, AND JAMES F. PRICE

Woods Hole Oceanographic Institution, Woods Hole, Massachusetts

(Manuscript received 25 July 2005, in final form 7 April 2006)

ABSTRACT

The overflow of dense water from the Nordic Seas through the Faroe Bank Channel (FBC) has attributes suggesting hydraulic control—primarily an asymmetry across the sill reminiscent of flow over a dam. However, this aspect has never been confirmed by any quantitative measure, nor is the position of the control section known. This paper presents a comparison of several different techniques for assessing the hydraulic criticality of oceanic overflows applied to data from a set of velocity and hydrographic sections across the FBC. These include 1) the cross-stream variation in the local Froude number, including a modified form that accounts for stratification and vertical shear, 2) rotating hydraulic solutions using a constant potential vorticity layer in a channel of parabolic cross section, and 3) direct computation of shallow water wave speeds from the observed overflow structure. Though differences exist, the three methods give similar answers, suggesting that the FBC is indeed controlled, with a critical section located 20–90 km downstream of the sill crest. Evidence of an upstream control with respect to a potential vorticity wave is also presented. The implications of these results for hydraulic predictions of overflow transport and variability are discussed.

1. Introduction

The qualitative resemblance of deep ocean overflows to dam or weir flows suggests that the former could be subject to hydraulic control. This process could be important in regulating the volume transport of the overflow and the stratification and circulation in the upstream basin. Because of the existence of a direct relationship between transport and upstream basin stratification, controlled flows should be easier to monitor than flows lacking control. Rotating hydraulic theory has suggested strategies for long-term monitoring based on upstream instrumentation (e.g., Helfrich and Pratt 2003; Hansen et al. 2001; Killworth and MacDonald 1993), but each of these theories requires a controlled flow in order to be valid.

In many cases the primary evidence for hydraulic control is the "overflow" character itself, the spillage of

dense fluid across the sill and the corresponding drawdown of isopycnals across the sill. Although this upstream–downstream asymmetry is suggestive, there are examples of similar behavior in noncontrolled flows, resulting from dissipation (e.g., Pratt 1986, Fig. 6). It is therefore important to get quantitative confirmation of control in terms of identification of the required subcritical-to-supercritical transition. Such confirmation has not generally been made in major overflows such as those of the Denmark Strait and Faroe Bank Channel. Should control be confirmed, it becomes important to know the location of the "critical" or "control" section where subcritical-to-supercritical transition takes place. This information is used in the formulation of the transport relation used for upstream monitoring. Transport relations (or weir formulas) applied in the past (e.g., Whitehead 1998; Nikolopoulos et al. 2003) assume that the control section lies at the crest of the sill, but this need not be the case. The lack of quantitative confirmation of hydraulic control and identification of the control section is due in part to the inability of hydraulic theory (see the review of Pratt 2004) to come to grips

Corresponding author address: James B. Girton, APL/UW, 1013 NE 40th Street, Seattle, WA 98105-6698.
E-mail: girton@apl.washington.edu

with the complications that arise in the presence of strong rotation (i.e., channel widths a significant fraction of the baroclinic Rossby radius or wider). In plain terms, nobody has been able to write down a generalized Froude number that can measure the hydraulic criticality of an overflow in a channel with arbitrary topographic cross section and account for the cross-stream variations in layer thickness, velocity, and potential vorticity that commonly occur. The development of such a measure would be a significant advance, even were it restricted to a single-layer, inviscid, reduced gravity approximation of the overflow.

The companion paper that precedes this contribution (Pratt and Helfrich 2005, hereinafter PH05) lays out several methods for assessing the hydraulic criticality of an observed overflow at a given section. The methodology assumes that the overflow can be reasonably approximated as a single layer with reduced gravity and a well defined interface. Entrainment and bottom drag are allowable so long as they enter the momentum and continuity equations as terms that lack derivatives, the quadratic drag law being one example. Application generally requires knowledge of the density structure across the flow, so that an interface can be defined, and is pinned on the assumption that the along-strait component of the velocity is geostrophically balanced. Although nothing as simple as a generalized Froude number is forthcoming, the methodology is straightforward.

We will apply the criteria laid out in PH05 to the deep flow through the Faroe Bank Channel (FBC), an overflow that has often been described in hydraulic terms (Borenäs and Lundberg 1988, 2004; Lake et al. 2005). This deep passage has recently been the subject of an observational program (Fig. 1) collecting high resolution sections of temperature, salinity, velocity, and dissolved oxygen along the FBC overflow path (Mauritzen et al. 2005). See also Prater and Rossby (2005) for a discussion of bottom-following float trajectories from this region. In this paper we describe the recently proposed methods for evaluating the hydraulic criticality of oceanic overflows, together with the application of these methods to the FBC dataset.

2. FBC

With its confined channel geometry, strong density contrast, and two-layer exchange flow, the FBC is a particularly likely candidate for hydraulic control among large-scale overflows. A density section along the center of the overflow (Fig. 2) shows a gradual isopycnal tilt approaching the sill (with the crest located at 0 km in the figure) followed by a dramatic steepening as the flow descends into the Iceland Basin to the left. At the same time, the dense layer (which we define

here as $\sigma_\theta > 27.65$ following Mauritzen et al. (2005)) thins and spreads, becoming a broad plume banked against the right-hand slope (Figs. 3 and 4).

Though an overall gravitationally driven character is clearly apparent, section and plan views (Figs. 3 and 4) both show substantial variations in the cross-stream direction, including a mean isopycnal tilt corresponding to the geostrophic velocity and thickness variations due to irregular topography. As the flow approaches the sill crest (section D) there is a suggestion of developing anticyclonic shear as might be produced by potential vorticity conservation in a thinning layer, however Lake et al. (2005) have documented appreciable variations in potential vorticity across the flow. Together these aspects make it difficult to define bulk properties, particularly layer thickness, to use when describing the flow as a whole.

3. Overflow criticality, method 1: Local Froude numbers

For a one-dimensional, single-layer flow with velocity V, layer thickness D, and reduced gravity g', the hydraulic state is described by the common Froude number $F = V/\sqrt{g'D}$. The flow is subcritical, critical, or supercritical according to $F < 1$, $F = 1$, or $F > 1$, respectively, and the expectation for a hydraulically controlled flow is $F < 1$ and $F > 1$ upstream and downstream, respectively, of the controlling sill. The critical or control section at which the subcritical-to-supercritical transition takes place generally coincides with the crest of the sill, though this location can be shifted elsewhere, usually downstream, as a result of bottom drag or entrainment (Pratt 1986; Gerdes et al. 2002). As discussed by PH05, the hydraulic criticality of a rotating channel flow is measured by the ability of a long wave, usually of the Kelvin type, to propagate upstream. The wave speed depends on the whole cross section of the flow and the side-wall boundary conditions, so it is the entire cross section that must be judged subcritical or supercritical. The common or "local" Froude number F typically varies across the flow and its value at any particular point is not an indication of the overall hydraulic state.

a. Layer-averaged velocity and density

To calculate F in a continuously stratified setting, g' and V must be suitably defined. One logical choice is

$$V = \frac{\left[\int_h^{h+D} v(z)\,dz\right]^2 + \left[\int_h^{h+D} u(z)\,dz\right]^2}{D^2} \quad \text{and}$$
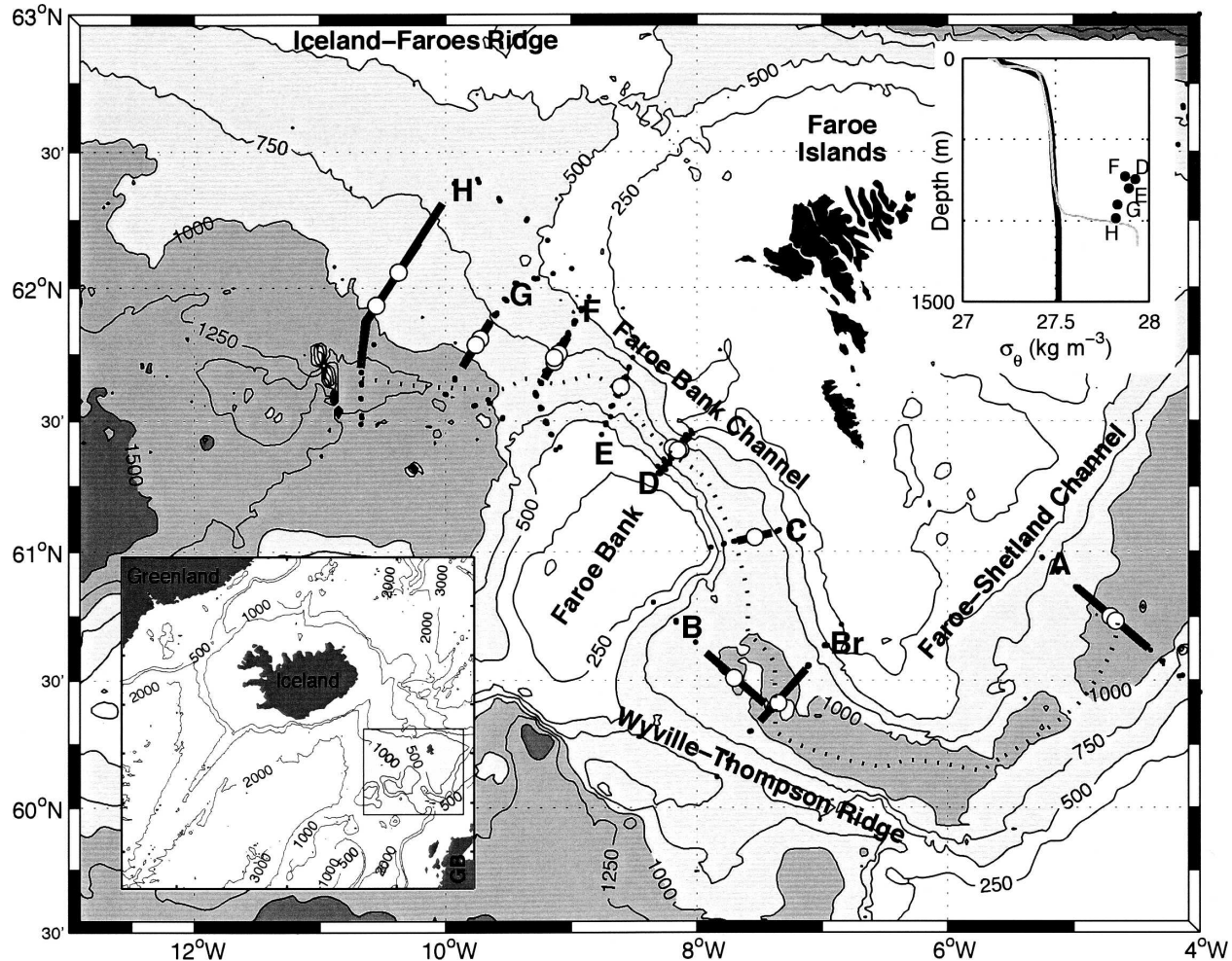
$$g' = \frac{g}{\rho D}\int_h^{h+D} \rho'(z)\,dz,$$

FIG. 1. Path of the dense overflow through the FBC. Open circles mark the center of mass anomaly of the dense layer during each section occupation, with section locations labeled A–H following Mauritzen et al. (2005). Gray bars show the width containing half of that anomaly. Black dots show station locations. Bathymetry is from Smith and Sandwell (1997), with *thalweg* path shown as a dotted line. Bottom left inset shows the measurement location on the Greenland–Scotland ridge. Top right inset shows the density profile of the background Atlantic Water (thick black line) along with mean overflow plume density vs depth for sections D through H (dots) and a single typical overflow density profile from section H (gray line).

where u and v are perpendicular components of velocity, ρ' is the density anomaly relative to the ambient stratification in the downstream basin (Fig. 1 inset), and h is the height of the bathymetry. In the FBC case, a single isopycnal appears reasonable to define the layer because of the sharp interfacial stratification and weak background stratification. Additionally, we usually define V as the magnitude of the layer average velocity.

As argued by PH05 based on the energy flux in long wave channel modes, a sufficient condition for the flow to be supercritical is that $F > 1$ all across the section in question (for any D, h, and unidirectional V distribution). However, this condition does not occur at any of the observed sections. Additionally, there is an expectation that critical flow will have values of F on either

side of unity as the section is crossed. This at least is a property of all known examples and has been proven for a channel with rectangular cross-section and unidirectional flow by Stern (1974). Application of this condition is somewhat problematic; even at a highly subcritical section with sluggish flow and very low interior values of F, the latter may rise above unity near the edges of the current because of the vanishing of D. It seems reasonable then to disqualify from the ranks of possible critical sections those over with $F > 1$ only close to the edges. As Fig. 4 shows, there are two sections, located 50 km (F) and 90 km (G) downstream of the crest of the sill, where F falls above and below unity near the left-hand side but away from the edges. These are the strongest candidates for control sections. Note
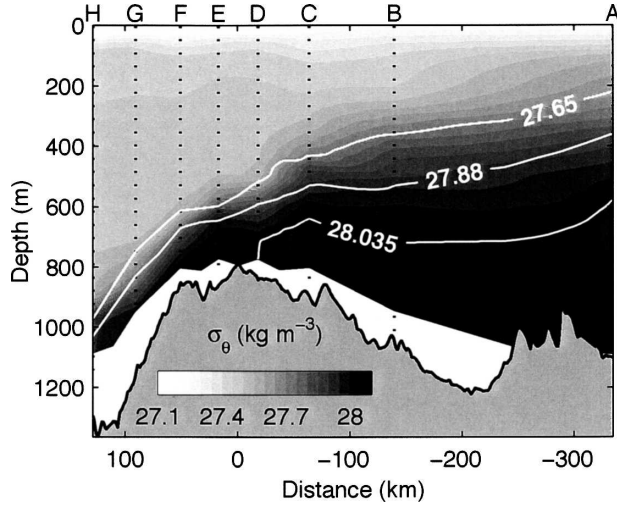
FIG. 2. Along-overflow density σ_θ section constructed from stations in the overflow core on the first occupation of each section in Fig. 1. Dense layer flow is from right to left, from the Nordic Seas into the Atlantic proper. The bottom topography along the deepest part of the channel (*thalweg*) is shaded gray, while the region below the bottom at each station selected is shaded white. Selected density contours for layers described by Mauritzen et al. (2005) are indicated in white.

that F falls well under unity across the sill crest suggesting subcritical flow there.

b. Modification for shear and stratification

The Froude number F used so far is based on a layer formulation that does not take into account the vertical variations of velocity and density within the moving layer. Nielsen et al. (2004) have shown that the neglect of vertical shear leads to an underestimation of inertial effects in the horizontal momentum equation, whereas the neglect of density variations leads to an overestimation of g'. Their work suggests that these effects can be compensated for by redefining the Froude number as $(\alpha/\beta)^{1/2}F$, where

$$\alpha = \frac{\int_h^{h+D} v(z)^2 \, dz}{DV^2} \geq 1 \qquad (1)$$

and

$$\beta = \frac{2\int_h^{h+D} \int_z^{h+D} \rho' \, dz' \, dz}{D^2 \overline{\rho'}} \leq 1 \qquad (2)$$

to account for vertical variations in v and ρ'. The criterion for control is then $F^2 = \beta/\alpha$, which Nielsen et al. (2004) verified analytically under the assumption of self-similar velocity and density profiles (i.e., constant or slowly varying α and β) and numerically with simu-
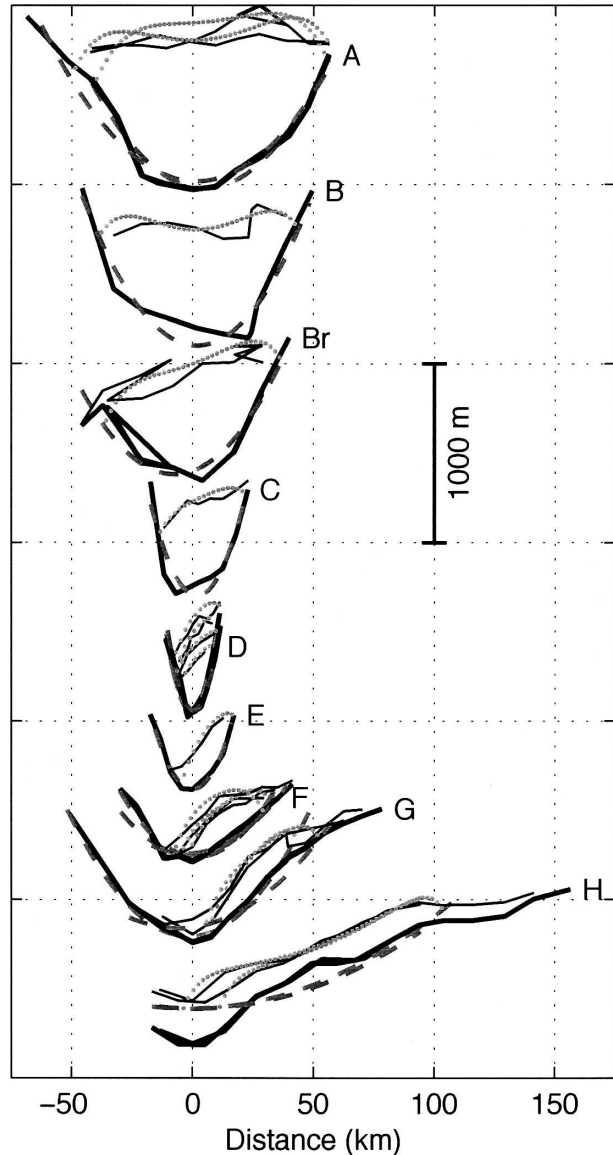

FIG. 3. Cross-section profiles of bathymetry (thick black lines), $\sigma_\theta = 27.65$ isopycnal interface (thin black lines), and parabolic model fits to the bathymetry (dashed gray lines) and interface (dotted gray lines) at each section. Note that sections B, Br, C, and E include only a single occupation, while A, G, and H include two occupations, F includes three occupations, and D includes four occupations. Even during single occupations, temporal variability is evident in the zigzag character of the interface during backtracks (A, Br) or pauses (B, G) in the sampling. Section Br ends at the Wyville–Thompson ridge, where a small amount of intermittent spillover is evident, though the principal direction of flow is perpendicular to the section (into the page).

lations of the propagation of small disturbances in a nonrotating stratified shear flow with internal friction.

The effective Froude numbers $(\alpha/\beta)F$ (always larger than F) are shown in Fig. 5, shaded according to transport VD. Though the shape coefficients α and β act to
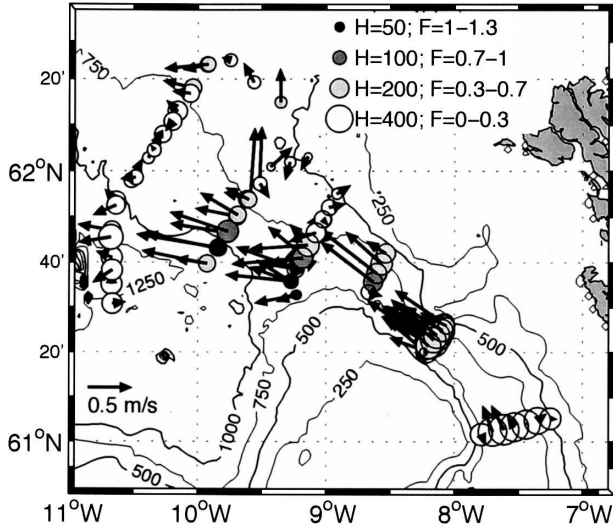
FIG. 4. The $\sigma_\theta > 27.65$ layer mean velocity (arrows), thickness (circle size), and local Froude number (circle shading). Each circle and arrow represent a single occupation of a station, so repeat stations (e.g., near the sill crest at section D) show many arrows superimposed, giving an impression of the directional consistency of the flow. See Fig. 1 for section names.
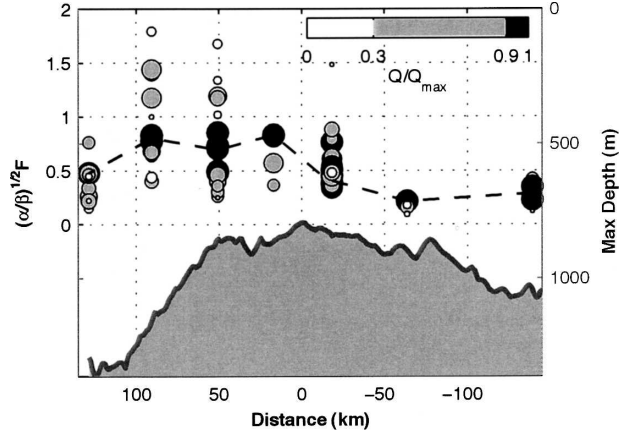

FIG. 5. All Froude numbers, incorporating stratification β and shear α coefficients, following Nielsen et al. (2004). Shading (and circle size) indicates the magnitude of local transport (vD) normalized for each section. Black indicates the overflow core (maximum transport), while white indicates the edges. The thick dashed line connects the core Froude numbers averaged over all occupations. The depth scale at right corresponds to the shading of the *thalweg* bathymetry. See Fig. 2 for section names.

increase the Froude number, they do not change the picture markedly from Fig. 4. Except in thin, highly sheared profiles at the edges of the flow, all values of α lie in the range 1–1.25 and all values of β lie in the range 0.8–1. The implications of Fig. 5 are of critical or supercritical flow 50–100 km downstream of the crest of the sill and subcritical elsewhere.

While the Nielsen et al. (2004) results, based on numerical simulations and similarity solutions, suggest that wave speeds are reduced in the presence of shear and stratification (so that the flow reaches criticality sooner), Garrett and Gerdes (2003) point out that inviscid waves in the presence of shear ought to be faster than their slab-flow counterparts, implying lower effective Froude numbers. Their formula produces even more scatter than shown in Fig. 5, but still suggests exclusively subcritical flow outside of the 50–100-km region and a few supercritical values within that region.

4. Overflow criticality, method 2: Parabolic channel

Rotating hydraulic theories have been developed for certain idealized flows and have resulted in the formulation of generalized Froude numbers. The theory that is the most flexible in its ability to deal with actual ocean topography is that of Borenäs and Lundberg (1986). The rotating channel has a parabolic cross section with the bottom elevation given by $h = h_0 + \alpha x^2$, x and y being the cross- and along-channel coordinates. Another restrictive assumption is that the potential vorticity $q = (f + \partial V/\partial x)/D$ of the flow is uniform. Direct velocity measurements are desirable in evaluating q because geostrophic calculation of $\partial V/\partial x$ would otherwise require two derivatives of the interface elevation $z = h + D$. The Froude number so obtained is

$$F_p^2 = \frac{T^2(x_a + x_b)^2}{(w - 2Tq^{-1/2})\{w - 2Tq^{-1/2} + (T^2 - 1)[w - (1 + 2\alpha)T\alpha^{-1}q^{-1/2}]\}}, \quad (3)$$

where $T = \tanh(wf/\sqrt{g'D_\infty})$, $D_\infty = f/q$, $w = x_a - x_b$, and x_a and x_b denote the positions of the edges of the flow. The value of F_p relative to unity measures the ability of a Kelvin wave to propagate upstream against the background flow. If $F_p > 1$ the wave is advected downstream by the current and the flow is supercritical,

at least with respect to this wave. This Froude number clearly differs from F in that it applies to the cross section of the flow as a whole.

Parabolic fits to the channel bathymetry and constant-potential vorticity (PV) layer fits to the interface are shown in Fig. 3. Additional information from mea-
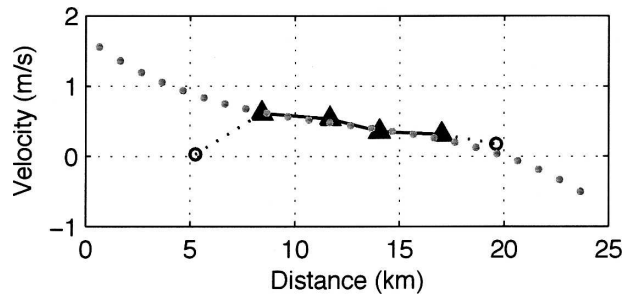
FIG. 6. Example of velocity fit to parabolic channel, constant-PV model at a single cross section (D). Black triangles indicate the measured along-channel velocity shear ($v_2 - v_1$) used in the fit. Gray dots indicate the best-fit constant-PV model profile. Open circles indicate unused velocity measurements (due to too-thin lower layer).
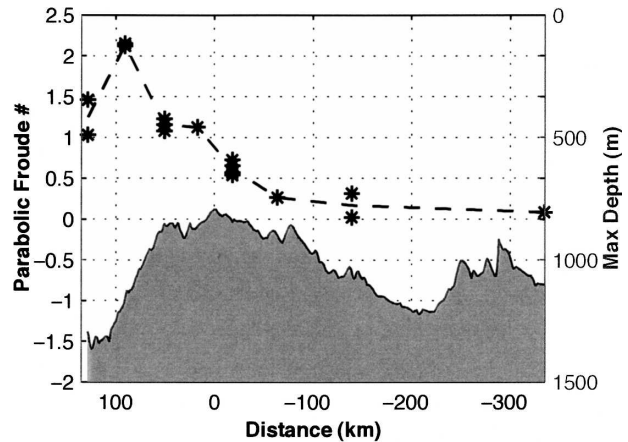

FIG. 7. Parabolic Froude number for each section. Note that the topography of the farthest downstream section (H) does not fit a parabola very well (Fig. 3), and so substantial subjectivity has been exercised in obtaining those numbers. See Fig. 2 for section names.

sured lateral shear (Fig. 6) was used to estimate D_∞ before fitting the interface. Notable discrepancies from a constant-PV structure are seen at the edges of the flow, where friction likely acts more rapidly than the lateral exchange of PV. Because of this, the model fitting of the velocity has been weighted by the layer thickness, resulting in a more accurate determination of the PV in the interior of the flow. In addition, downstream of the sill the bathymetry of the FBC opens into a broad slope, where fitting the cross section to a parabola becomes more problematic. For this reason, the section H results (130 km) are to be viewed with a healthy dose of skepticism.

Values of F_p from each overflow cross section are presented in Fig. 7. The flow is subcritical at section D but passes through a critical section shortly downstream, possibly at the sill crest itself. At 100 km downstream, the flow appears supercritical, however, substantial departures from a constant potential vorticity profile occur near the edges of these sections. This suggestion of a critical section close to the crest of the sill could be seen as verification of the expected hydraulic character of the overflow. However, the lack of local $F > 1$ in the same region points to possible problems with this interpretation.

Lake et al. (2005) have generated a 2-month time series of F_p in 1998 from three ADCP moorings at a location very close to section D. They found variability mostly in the range $0.6 < F_p < 1.1$, including two periods of subcritical flow, which they attribute to intensified upper-layer inflow velocities. These measurements are consistent with the near-sill values of F_p in Fig. 7.

5. Overflow criticality, method 3: Direct calculation of wave speeds

The most appropriate method of determining criticality is also the most difficult to implement. The direct

calculation of the long wave speeds based on the flow at a particular section determines whether disturbances can propagate upstream or not. Of the possible normal modes, Kelvin-like waves are arguably the most important. Overflows are driven by gravity and one would generally expect a controlling wave mode to be gravitational as well. However, rotating channel flows also admit a discrete spectrum of potential vorticity waves, and it is conceivable that they could play some role as well.

PH05 lay out a method for calculating the phase speeds based on knowledge of the interface shape and topography across a particular section of the deep channel. The method is based on dividing the observed flow into N discrete subsections or streamtubes and considering small perturbations of the position and elevation of the material edges of the streamtubes. The phase speeds c turn out to be the eigenvalues of a $2N \times 2N$ matrix as described in appendix D of PH05. To fit the streamtube model, one must choose N in accordance with the horizontal resolution of the measurements. The steps that have been taken to resolve the sill flow in terms of $N = 4$ streamtubes is illustrated in Fig. 8. First, the edges of the dense layer are determined by extrapolating the interface to intersect with the bathymetry. Next, the interface and bathymetry are both smoothed by fitting fifth-order polynomials. Last, the layer is divided into streamtubes of equal width. The resulting interface depth and bathymetry depth and slope at each streamtube boundary are fed into the matrix computation for the wave modes and speeds.

Figure 9 shows the vertical and lateral displacement structure for four of the section D wave modes as cal-
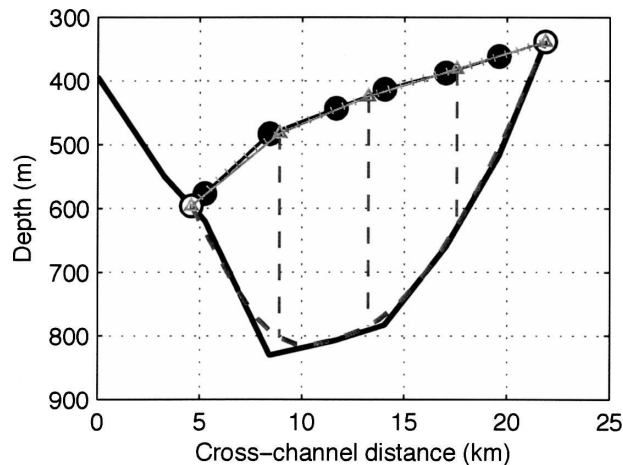
FIG. 8. Construction of multiple streamtube model parameters from data at section D. Thick black line and filled circles show the station bathymetry and interface position. Open circles indicate interpolated intersection points. Smoothed bathymetry (thick dashed gray line) and interface (dotted gray line) are interpolated to give four equal-width segments with boundaries indicated by vertical dashed lines.

culated using $N = 4$. The first wave (top left panel) is Kelvin-like: it has an interface displacement that is trapped on the left side of the channel. Its phase speed is negative, indicating upstream propagation. All of the other wave modes have positive speeds and these include potential vorticity (Rossby-like) modes and a right-wall trapped Kelvin mode (bottom right panel). The four additional potential vorticity modes also primarily involve lateral displacements in the streamtube edges (not shown). We conclude that the flow at the crest of the sill is subcritical with respect to Kelvin waves and supercritical with respect to potential vorticity waves.

Figure 10 shows the speeds of the waves calculated at all sections for $N = 4$. The range of c at each section is bounded above and below by the Kelvin wave speeds (solid lines). The lower value is negative at all the sections save the one lying 50 km downstream (F). There c is positive for one occupation and slightly less than zero for two other occupations. We conclude that the flow at this section is critical, or marginally critical with respect to Kelvin waves, and subcritical elsewhere. It is possible of course that undetected intervals of supercritical flow occur between the observed sections, but the predominance of subcritical conditions downstream of the critical point suggests a limiting behavior such as might be provided by shear instability and entrainment. This possibility will be discussed below.

For the potential vorticity waves, which have intermediate values of c, the flow is supercritical from 140 km upstream of the sill crest to all points downstream.

However there is one mode whose speed becomes negative upstream of this point, and the -140-km mark therefore appears to be a control point with respect to this potential vorticity wave.

6. Discussion and conclusions

A suite of tools now exists for diagnosing hydraulic criticality in rotating gravity current flows. The least conclusive measure involves the variation of the local Froude number F across the section in question and the expectation that it must fall above and below unity at a critical section. All sections have locations where $F < 1$, but only the two sections lying between 50 and 100 km downstream of the sill crest have values > 1. (We have excluded from this discussion the very high Froude numbers that may occur at the edges of the current.) This conclusion holds whether or not F is corrected for the presence of vertical shear and continuous density variations.

More definitive is the parabolic Froude number F_p, which is observed to pass through unity at or slightly downstream of the sill crest and to remain >1 thereafter. The most problematic aspect of this measure is the lack of fit between the assumed constant PV profile and the actual interface and velocity profiles in the sections lying 50–150 km downstream. Particularly unsatisfying is the lack of fit at the left edge of the flow, where an upstream propagating Kelvin wave would be trapped.

The most conclusive measure is the direct long-wave speed calculation, which suggests a Kelvin wave control approximately 50 km downstream of the sill crest, where the bottom slope suddenly increases (Fig. 10). Although the Kelvin wave speed c is formally positive here for only one occupation of the section, the relatively low absolute value of the c for the other occupation, when c is slightly negative, suggests a control nearby.

In summary the FBC overflow appears to be controlled, though only marginally so, at a section 20–90 km downstream of the sill crest. Time variability could mean that the actual control section is not stationary. The lack of Froude numbers (of any type) that far exceed unity and would thereby indicate hydraulic control in a more decisive way can be explained as follows. It is well known that in nonrotating, one-dimensional applications, bottom drag tends to drive Froude number toward unity and thereby limits large values of F from occurring over downslopes. Gerdes et al. (2002) have also shown that the same effect occurs as a result of the momentum fluxes produced when the overflow entrains quiescent fluid from above. A closely related process is the mixing of momentum that occurs as the re-
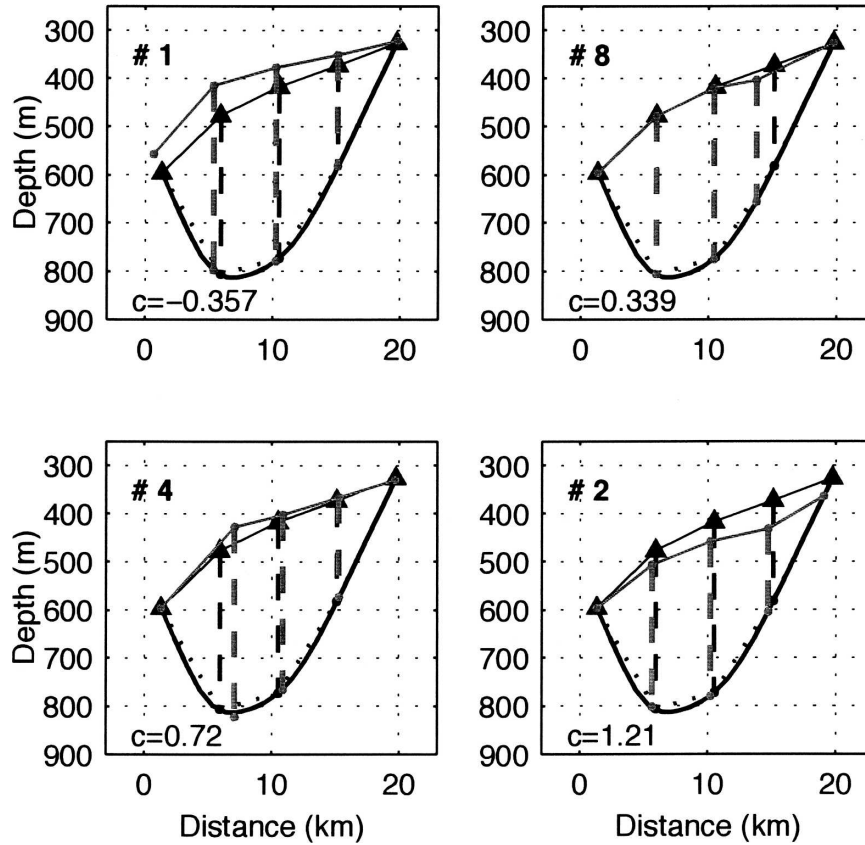
FIG. 9. Wave structure eigenvectors at section D. Perturbed positions of the plume interface and streamtube boundaries are indicated by gray lines for the two fastest upstream- and downstream-propagating waves. The wave speed c is indicated for each eigenvector, with $c < 0$ indicating a wave that is able to propagate upstream. Black lines and symbols, identical in each panel, show the rest-state interface, streamtube boundary positions, and bathymetry. Note that an actual wave could have any (small) amplitude and would alternate between the perturbation structure shown and one of the opposite sign.

sult of interfacial instabilities triggered when F exceeds unity (Price and Baringer 1994). All of these factors limit the extent to which F can exceed unity in a flow with bottom drag and entrainment producing instabilities. Although some of these conclusions are based on one-dimensional models that lack rotation, we generally expect something of the same nature in the present application.

Inviscid hydraulic theory would require that the control section lie at the crest of the sill, so its downstream location must be a consequence of nonconservative processes such as bottom drag and entrainment. A crude estimate of the true position can be made based on a nonrotating hydraulic theory that accounts for quadratic bottom drag as well as a vertical entrainment velocity.

As shown by Gerdes et al. (2002) and Pratt (1986), the control section lies where

$$\frac{dh}{dy} = -C_d - \frac{3}{2}\frac{w_e}{V} + \frac{D}{W}\frac{dW}{dy}, \qquad (4)$$

where C_d is the dimensionless quadratic drag coefficient, estimated at 4×10^{-3} from the relationship between 10-m velocity and log-layer bottom stress in the FBC (Mauritzen et al. 2005).[1] Here, w_e is the positive downward entrainment velocity, and W is the channel width. Inferring w_e/V from the dilution of the density anomaly in the descending overflow (as in Girton and Sanford 2003) gives a value of 5×10^{-4} (with at least a factor of 2 uncertainty). The gradual widening of the plume between sections D and G leads to an estimate

---

[1] This estimate of C_d is about a factor of 10 greater than reported by Duncan et al. (2003) from somewhat similar stress and velocity data. We believe that the difference arises from an error in the Duncan et al. (2003) definition of the drag coefficient.
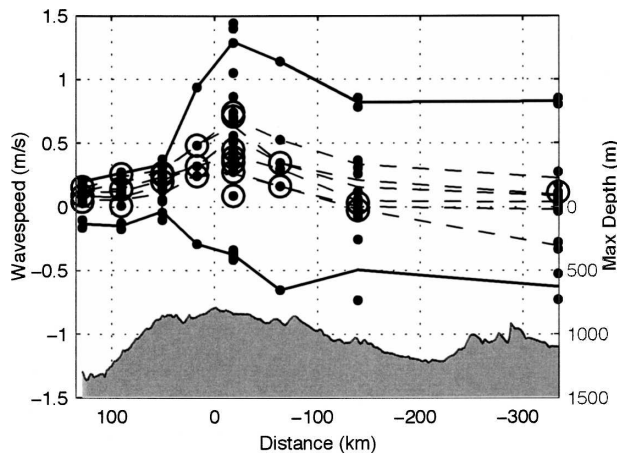
FIG. 10. Wave speeds vs distance for multiple-streamtube model with $N = 4$. Dots indicate all eight wave speeds computed for each section, including multiple occupations. Solid lines indicate the maximum and minimum wave speeds averaged over all occupations. Dashed lines indicate intermediate wave speeds averaged over all occupations. Open circles indicate wave speeds with non-zero imaginary parts.

of $D/W(dW/dy)$ on the order of 1×10^{-3}. Thus, the second and third terms on the right-hand side of (4) essentially cancel, implying that frictional effects should push the control section downstream to where the slope along the axis of the overflow is 4×10^{-3}. This can only be achieved in the vicinity of the 50-km section, where the slope increases rapidly from less than 2×10^{-3} to at least 5×10^{-3} (Fig. 2).

One way to estimate the consequence of a shift in the position of the control section away from the sill crest is by considering the Whitehead et al. (1974) formula for the volume flux of a rotating hydraulically controlled overflow:

$$Q = \frac{g'\Delta z^2}{2f}, \qquad (5)$$

where Δz is the elevation difference between the sill and the interface in a hypothetical quiescent upstream basin. The model is highly idealized in its assumptions of zero potential vorticity and rectangular cross section, but it will serve to produce an estimate. We note that subsequent work (e.g., Helfrich and Pratt 2003) has shown (5) to be applicable to flow with arbitrary potential vorticity, provided that the flow at the sill is separated and that Δz is measured along the right-hand wall of the rectangular channel (facing downstream).

For the FBC, Whitehead (1998) used $\Delta z = 400$ m, which gives a transport of 3.0 Sv. This value may be compared with the 2.3 Sv observed by Lake et al. (2005) during "controlled periods" and the 2.4 Sv observed at

the sill in the current dataset (Mauritzen et al. 2005). The theoretical overestimate might be because a rectangular cross section is assumed within a channel, whereas the more realistic rounded cross section is known to reduce the transport (Borenäs and Lundberg 1988; estimate a 25%–30% reduction using a parabolic cross section). Suppose that the critical section does indeed lie 50 km downstream, where the minimum bottom elevation is 50 m lower that at the crest of the sill. Increasing Δz by 50 m leads to an increase in the predicted transport of about 25%. However, this is not the full story. Among the assumptions used to derive (5) is that entrainment and bottom drag can be ignored, whereas these effectively reduce Δz. This reduction is difficult to estimate with any precision, but the energy loss to bottom drag alone, considered over the $L = 50$ km distance between the sill crest and the actual control, and with a mean velocity V, depth D, and drag coefficient C_d, would cause Δz to be reduced by an amount roughly equal to $C_d L V^2/(g'D)$. Using $C_d = 4 \times 10^{-3}$ and $V/\sqrt{g'D}$ in the range 0.4–0.8, we get estimates of Δz reduction between 32 m and 128 m. In other words, dissipation is likely to more than compensate for the drop in elevation of the critical section and may be at least partially responsible for the overestimate of transport by (5). There is a clear need to pursue these ideas further using a more sophisticated model. When benchmarked by the roughly 30% decrease in the FBC overflow thought to have occurred over the past half century (Hansen et al. 2001) the shift in the control section is certainly worth accounting for.

Two of our three methods have indicated that much of the outflow "plume" is hydraulically subcritical, a property that would render the flow sensitive to downstream information. This aspect could have implications for streamtube models (Smith 1975; Killworth 1977; Price and Baringer 1994), which are often used to simulate plumes. An essential approximation made by all such models is that the outflow is sufficiently thin that the interface parallels the bottom and thus the pressure gradient is proportional to the bottom slope. A consequence is that gravity waves are expunged from the model and upstream propagation of information is disallowed. The extent to which this is a problem for streamtube models of the Faroe Bank outflow is not known.

Another unresolved issue raised by the analysis is the possible presence of an apparent control section with respect to potential vorticity waves 140 km upstream of the sill (see Fig. 10). As discussed in the review by Johnson and Clarke (2001), Rossby wave control generally involves horizontal structure rather than interfacial dynamics. Pratt and Armi (1987) explored a chan-

nel model that contains gravity (interfacial) and potential vorticity dynamics. Flow states with potential vorticity controls tend to contain lateral counterflows and recirculations. Pratt and Armi (1987) also observed that such a flow cannot be joined smoothly and conservatively to a flow with a gravity wave control. While suggestions of dense-layer flow recirculations in the Faroe–Shetland Channel have been reported, these features are difficult to separate from the strong tidal and upper-layer eddy variability in the same region (see Hosegood et al. 2005; Sherwin et al. 2006). The subject certainly warrants further study.

REFERENCES

Borenäs, K., and P. Lundberg, 1986: Rotating hydraulics of flow in a parabolic channel. *J. Fluid Mech.,* **167,** 309–326.

——, and ——, 1988: On the deep-water flow through the Faroe Bank Channel. *J. Geophys. Res.,* **93,** 1281–1292.

——, and ——, 2004: The Faroe-Bank Channel deep-water overflow. *Deep-Sea Res. II,* **51,** 335–350.

Duncan, L. M., H. L. Bryden, and S. A. Cunningham, 2003: Friction and mixing in the Faroe Bank Channel outflow. *Oceanol. Acta,* **26,** 473–486.

Garrett, C., and F. Gerdes, 2003: Hydraulic control of homogeneous shear flows. *J. Fluid Mech.,* **475,** 163–172.

Gerdes, F., C. Garrett, and D. Farmer, 2002: On internal hydraulics with entrainment. *J. Phys. Oceanogr.,* **32,** 1106–1111.

Girton, J. B., and T. B. Sanford, 2003: Descent and modification of the overflow plume in the Denmark Strait. *J. Phys. Oceanogr.,* **33,** 1351–1364.

Hansen, B., W. R. Turrell, and S. Østerhus, 2001: Decreasing overflow from the Nordic seas into the Atlantic Ocean through the Faroe Bank Channel since 1950. *Nature,* **411,** 927–930.

Helfrich, K. R., and L. J. Pratt, 2003: Rotating hydraulics and upstream basin circulation. *J. Phys. Oceanogr.,* **33,** 1651–1663.

Hosegood, P., H. van Haren, and C. Veth, 2005: Mixing within the interior of the Faeroe-Shetland Channel. *J. Mar. Res.,* **63,** 529–561.

Johnson, E. R., and S. R. Clarke, 2001: Rossby wave hydraulics. *Annu. Rev. Fluid Mech.,* **33,** 207–230.

Killworth, P. D., 1977: Mixing on the Weddell Sea continental slope. *Deep-Sea Res.,* **24,** 427–448.

——, and N. R. MacDonald, 1993: Maximal reduced-gravity flux in rotating hydraulics. *Geophys. Astrophys. Fluid Dyn.,* **70,** 31–40.

Lake, I., K. Borenäs, and P. Lundberg, 2005: Potential-vorticity characteristics of the Faroe Bank Channel deep-water overflow. *J. Phys. Oceanogr.,* **35,** 921–932.

Mauritzen, C., J. Price, T. Sanford, and D. Torres, 2005: Circulation and mixing in the Faroese channels. *Deep-Sea Res. I,* **52,** 883–913.

Nielsen, M. H., L. Pratt, and K. Helfrich, 2004: Mixing and entrainment in hydraulically driven stratified sill flows. *J. Fluid Mech.,* **515,** 415–443.

Nikolopoulos, A., K. M. Borenäs, R. Hietala, and P. Lundberg, 2003: Hydraulic estimates of Denmark Strait overflow. *J. Geophys. Res.,* **108,** 3095, doi:10.1029/2001JC001283.

Prater, M. D., and T. Rossby, 2005: Observations of the Faroe Bank Channel overflow using bottom-following RAFOS floats. *Deep-Sea Res. II,* **52,** 481–494.

Pratt, L. J., 1986: Hydraulic control of sill flow with bottom friction. *J. Phys. Oceanogr.,* **16,** 1970–1980.

——, 2004: Recent progress on understanding the effects of rotation in models of sea straits. *Deep-Sea Res. II,* **51,** 351–369.

——, and L. Armi, 1987: Hydraulic control of flows with non-uniform potential vorticity. *J. Phys. Oceanogr.,* **17,** 2016–2029.

——, and K. R. Helfrich, 2005: Generalized conditions for hydraulic criticality of oceanic overflows. *J. Phys. Oceanogr.,* **35,** 1782–1800.

Price, J. F., and M. O. Baringer, 1994: Outflows and deep water production by marginal seas. *Progress in Oceanography,* Vol. 33, Pergamon, 161–200.

Sherwin, T. J., M. O. Williams, W. R. Turrell, S. L. Hughes, and P. I. Miller, 2006: A description and analysis of mesoscale variability in the Färoe-Shetland Channel. *J. Geophys. Res.,* **111,** C03003, doi:10.1029/2005JC002867.

Smith, P. C., 1975: A streamtube model for bottom boundary currents in the ocean. *Deep-Sea Res.,* **22,** 853–873.

Smith, W. H. F., and D. T. Sandwell, 1997: Global sea floor topography from satellite altimetry and ship depth soundings. *Science,* **277,** 1956–1962.

Stern, M. E., 1974: Comment on rotating hydraulics. *Geophys. Fluid Dyn.,* **6,** 127–130.

Whitehead, J. A., 1998: Topographic control of oceanic flows in deep passages and straits. *Rev. Geophys.,* **36,** 423–440.

——, A. Leetmaa, and R. A. Knox, 1974: Rotating hydraulics of strait and sill flows. *Geophys. Fluid Dyn.,* **6,** 101–125.